ELSEVIER

International Journal of Pressure Vessels and Piping 76 (1999) 803–811

INTERNATIONAL JOURNAL OF
Pressure Vessels and Piping

www.elsevier.com/locate/ijpvp

Failure correlation between cylindrical pressurized vessels and flat plates

E.S. Folias*

Department of Mathematics, University of Utah, Salt Lake City, UT 84112, USA

Received 25 March 1999; accepted 11 April 1999

Abstract

Utilizing the theory of thin shell structures, a failure criterion is presented which one may use to predict, analytically, catastrophic failures, or unzipping, in cylindrical pressurized vessels, based on the fracture toughness profile K obtained from tests carried out on flat plates of the same material and thickness. These test results are plotted as a function of the characteristic ratio (h/c), where h represents the specimen thickness and c one-half of the crack length. Comparison with carefully controlled experimental data substantiates its validity and its potential use. The advantage of such an approach is that considerable amount of time and money can be saved. © 1999 Elsevier Science Ltd. All rights reserved.

Keywords: Thin shell structures; Fracture toughness; Flat plates; Cylindrical vessels; Fracture

1. Introduction

In nature, shells are the rule than the exception. The list of natural shell-like structures is long, and the strength properties of some of them are remarkable. It is logical, therefore, for man to utilize them in man-made structures. But to do this safely, we must understand the fundamental laws that govern the strength and displacement behavior of such structures for they are not immune to failures, particularly in the fracture mode.

The engineering community has long recognized that large, thin-walled, pressurized cylindrical vessels resemble balloons and like balloons are subject to puncture and explosive loss. For a given material, under a specified stress field due to an internal pressure q_0, there will be a crack length in the material which will be self-propagating. Crack lengths less than the critical value will cause leakage but not destruction. However, if the critical crack length is ever reached, either by penetration or by the growth of a small fatigue crack, explosion and complete loss of the structure may occur. Therefore, to ensure the integrity of the structure, the designer must be cognizant of the relationship that exists between fracture load, flaw shape and size, material properties, and global cylindrical geometry. A relationship of this kind is referred to as a fracture criterion and can be derived by the application of the theory of fracture mechanics.

2. General theory

Let us consider a portion of a thin, shallow cylindrical vessel, of constant thickness h, which is subjected to a uniform internal pressure q_0 and contains a through-the-thickness crack of length $2c$. In this paper, we shall limit our considerations to elastic, isotropic and homogeneous segments of cylindrical vessels that are subjected to small deformations.

The basic variables in the theory of cylindrical pressurized vessels are, the displacement function $W(x,y)$ in the direction of the z-axis, and the stress function $F(x,y)$ which represents the stress resultants tangent to the middle surface of the shell. Following Marguerre (1938), the differential equations governing W and F, with x and y the rectangular Cartesian coordinates of the base plane (see Fig. 1) are given by:

$$\nabla^2 F + \frac{Eh}{R}\frac{\partial^2 w}{\partial x^2} = 0, \tag{1}$$

$$\nabla^2 W - \frac{1}{RD}\frac{\partial^2 F}{\partial x^2} = \frac{q_0}{D} \tag{2}$$

where ∇^4 is the biharmonic operator, E the Young's modulus, h the thickness of the vessel, D the flexural rigidity, and q_0 the internal pressure.

For a cylindrical vessel, three observations are worth noting. First, the coupled nature of the differential equations clearly suggests that there exists an interaction between bending and stretching. That is, a bending load will

* Tel.: + 1-801-581-6851; fax: + 1-801-581-4148.

PII: S0308-0161(99)00045-9

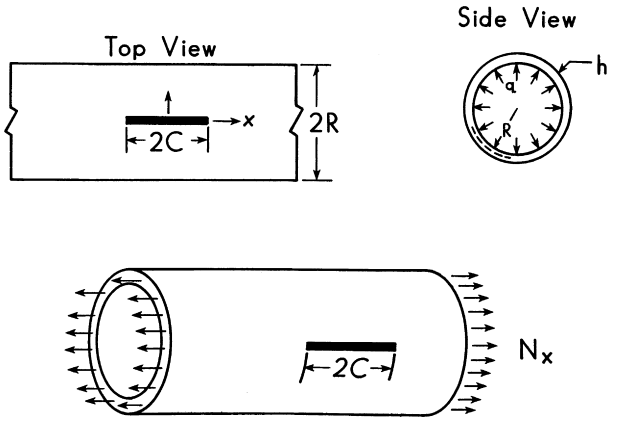

Fig. 1. Geometry and coordinates of an axially cracked cylindrical vessel.

generally induce both bending and extensional stresses, and similarly a stretching load will also induce both bending and extensional stresses. Second, the radius of curvature varies all the way from zero to a constant as one sweeps from the axial to the peripheral direction. Third, if one lets the cylinder radius R to tend to infinity, the special case of a flat plate is recovered.

Theoretical investigations of the above equations in the presence of discontinuities such as cracks have been carried out by Folias (1964,1974), Copley and Sanders (1969), Erdogan and Kibler (1969). Moreover, Folias [1,2] was able to show that there exists a correlation function between a cylindrical pressure vessel and the corresponding case of a flat plate, i.e.

$$\sigma_{\text{cylinder}} = \{1 + f\}^{-1/2}\sigma_{\text{plate}} \tag{3}$$

where the function f represents a geometrical correction factor

$$f = 0.317\lambda^2 \tag{4}$$

and

$$\lambda^2 = \{12(1 - \nu^2)\}^{1/2}\frac{c^2}{Rh}. \tag{5}$$

Although this correlation function was derived on the basis of a homogeneous and isotropic material, the author believes that it reflects the dominant term of a geometrical inherent property that exists between shallow cylindrical shell structures and similarly loaded flat plates of the same material. Such a property is of great practical value for it may now be used to predict failing stresses in pressurized cylinders by simply performing experiments on flat plates. This represents a great advantage because (i) it is relatively easy to carry out experiments on flat plates and (ii) it is less expensive.

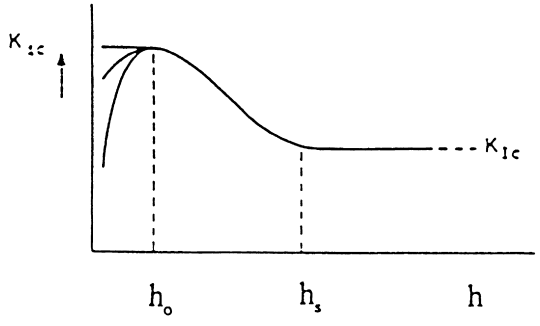

Fig. 2. Fracture toughness versus specimen thickness.

3. Analysis of tests carried out on flat plates

Recent tests data carried out by Royce Foreman and his group (NASA) on cracked plates may be found in Appendices A and B. These tests were carried out on flat plates, made of aluminum 2219-T87, in order to establish the fracture toughness curve, K. The material is to be used in the construction of the US space station Manned Module. These experimental data may now be used, in conjunction with the theory developed by Folias [2], to predict catastrophic failures in pressurized vessels of the same material. However, to accomplish this, one must examine the above experimental data from a slightly different point of view.

It has long been recognized by the fracture mechanics community that the fracture toughness curve is not really a material constant, and that its true value depends strongly on the specimen thickness. Its expected behavior may be seen schematically in Fig. 2. The reader may note that beyond a certain thickness h_s, a state of plane strain prevails whereby the toughness reaches the value of K_{Ic}. Alternatively, there exists an optimum thickness h_o, where the toughness reaches its highest value. This value is referred to as plane stress fracture toughness and its failure is characterized as *shear* or *slant* fracture. Moreover, for a thickness smaller than h_o there has, in the past, been some uncertainty about the toughness. In some cases, a horizontal level was found [3,4], while in other cases a decreasing toughness was observed [5–7]. It may also be noted that for a thickness $h < h_o$, the plastic zone is approximately equal to the specimen thickness and yielding in the thickness direction is unconstrained. As a result, a state of plane stress can fully develop in such regions. Presently, it is widely accepted that for $h < h_o$ the fracture toughness decreases almost linearly to the value of zero. Experimental evidence of this, for 7075-T6 aluminum alloy, is shown in Fig. 3 (see Ref. [8, p. 136]).

Additionally, recent 3D analytical studies on flat plates carried out by Folias and co-workers reveal that the stress concentration factor [9,10,15], as well as the stress intensity factor [11], are indeed functions of the radius to half-thickness ratio (a/h), and half-crack size to half-thickness ratio (c/h), respectively. Thus, motivated by these findings, we tabulate in Appendix C Foreman's experimental fracture toughness data as a function of the parameter (h/c), i.e. the thickness to half-crack size ratio.

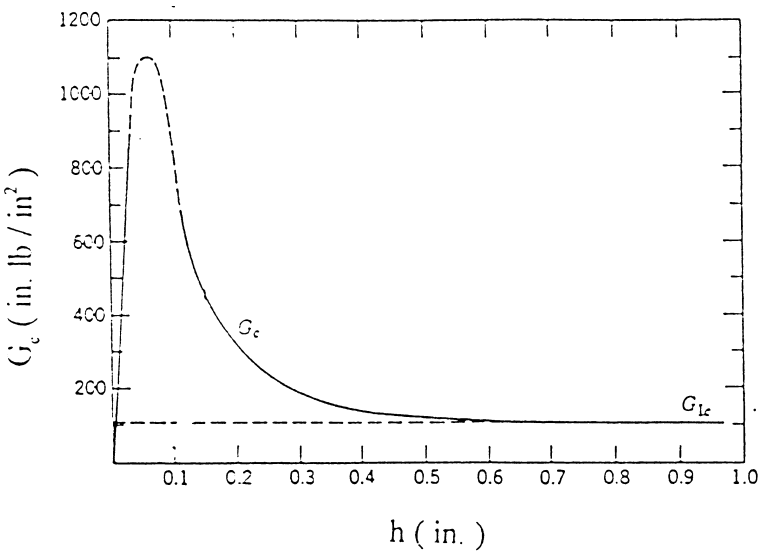

Fig. 3. Strain-energy release rate versus specimen thickness for 7075-T6 aluminum alloy.

A careful examination of Appendices A–C reveal the following observations to be worth noting:

1. For the ratio of $(h/c) = 0.047$, the variation of the fracture toughness reported was approximately 12%! (This is interesting particularly when the thickness, crack sizes and specimen widths were almost the same (see Appendix A, tests A). The variation suggests, perhaps, the presence of some sort of local material instability.)
2. Tests E, G and H do not appear to follow the expected trend. Apparently, something was different in this set of experiments that the author cannot speculate on and for this reason we will ignore (see Fig. 4).
3. Tests 2J, 2K and 2L were carried out on flat plates with a 0.08 in. thickness and appear to be in line with the expected trend.
4. Comparison between tests A and 2K show that, even though the ratio h/c is the same, and the ratio c/w is approximately the same, the values of the fracture toughness vary by 9%, which is in line with observation (1).

In view of the above, we conclude that an experimental scatter of approximately 10–12% is to be expected for this material.

4. The fracture toughness curve

Utilizing the data of the table in Appendix C, we now plot the experimental values of the fracture toughness K, as a function of the parameter (h/c) (see Fig. 4). The profile of the fracture toughness appears to follow the theoretically expected trend. Perhaps it is appropriate here to note that, this procedure works best if the experiments are carried out on flat plates of the same thickness. Unfortunately, the tests reported in Appendices A and B were carried out on flat plates with different thicknesses. Consequently, the reader may notice that tests A show a slightly higher rise than those of tests 2K. This occurs in the region that is characterized with a 45° plane fracture or more commonly referred to as *shear fracture*.

The reader may also notice that the thickness for the tests #A is $h = 0.191$ in. (see Appendix A), while the thickness for the test 2K is $h = 0.083$ in. (see Appendix B). This observation brings the following two questions to mind. Why is there a need for the presence of two different paths? Moreover, at what value of (h/c) does this bifurcation take place?

A partial answer to the above two questions may be obtained from the results of the work on the 3D stress field of a plate weakened by the presence of a circular hole [9]. Recently, utilizing a more sophisticated numerical analysis, these results have further been sharpened (Folias, 1997) and the maximum, 3D, stress concentration factor versus the radius to half-thickness ratio is shown in Fig. 5. The results of this figure provide us with a definite answer, at least for the case of a circular hole, of the regions in which a plate is considered to be in a state of plane stress, i.e. $a/h > 10$, or in a state of plane strain, i.e. for $a/h < 0.10$. Moreover, the transition region occurs between the values of $0.10 < a/h < 10$, whereby the 3D effects become more pronounced. Thus, if one assumes that similar trends also prevails in the case of a, 3D, cracked plate, one may conjecture that a state of plane stress exists for ratios of $h/c < 0.1$. This result appears to be in line with the experimental curves of Figs. 2 and 3. Further, it is also known that for $h < h_0$, the fracture toughness is proportional to $\sqrt{h\varepsilon_f}$. As a result, it is not unusual to have a fan, or a series of paths, for different thicknesses that fan out to the left of the critical ratio $h/c = 0.1$. Such conjecture, may also explain the experimental uncertainty noted by researchers in the past (see discussion of Fig. 2).

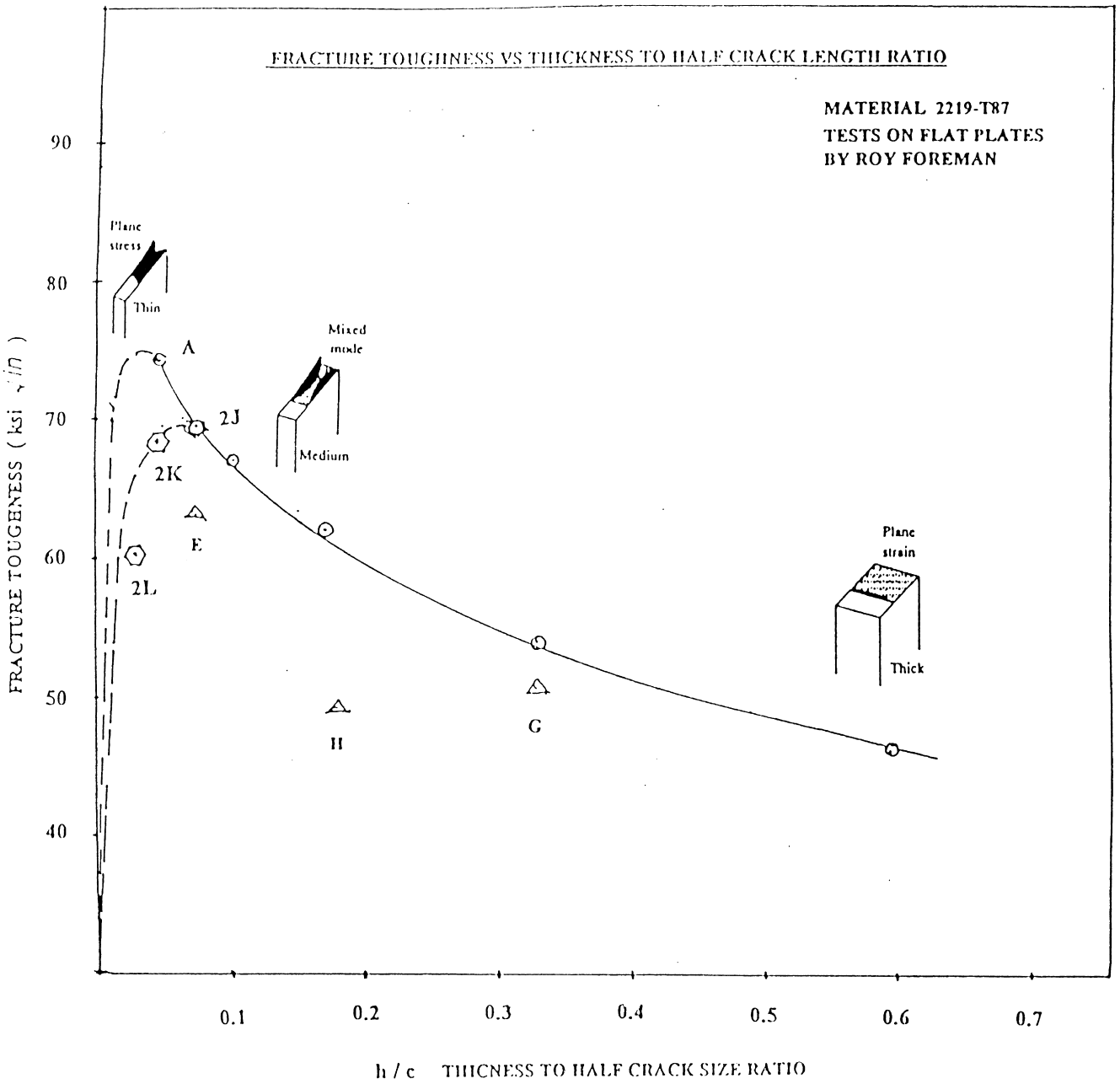

Fig. 4. Fracture toughness versus thickness to half crack length ratio for 2219-T87 aluminum alloy plates.

5. Failure prediction in pressurized vessels

The fracture toughness curve, as given by Fig. 4, may now be used to predict *the static* failing pressures in cylindrical vessels made of Al 2219-T87. For static considerations, the results by Folias [2] should be applicable. More specifically, under the assumption that bending and bulging effects are negligible, Folias's general failure criterion [2] may then be approximated by the simple relationship

$$\frac{q_0}{1000}\frac{R}{h}\sqrt{\pi c}\sqrt{1+0.317\lambda^2}=K, \tag{6}$$

where q_0 is expressed in psi. Alternatively, if the effects of bending and bulging are sufficiently large, then the approximate equation (6) can no longer be used and the general failure criterion must be utilized.

Recently, two very carefully controlled experiments on pressurized vessels were carried out by Nemat Nasser and his group at UCSD. The work was done in order to assess the structural characteristics of the United States Manned Module of the International Space Station. The tests were carried out on cylindrical pressurized vessels, of 20.75 in. diameter and for two different values of thickness, $h=$ 0.05 and 0.086 in, respectively. The cylinders were made out of Al 2219-T87.

A crack length of $2c=5.5$ in. was very cleverly

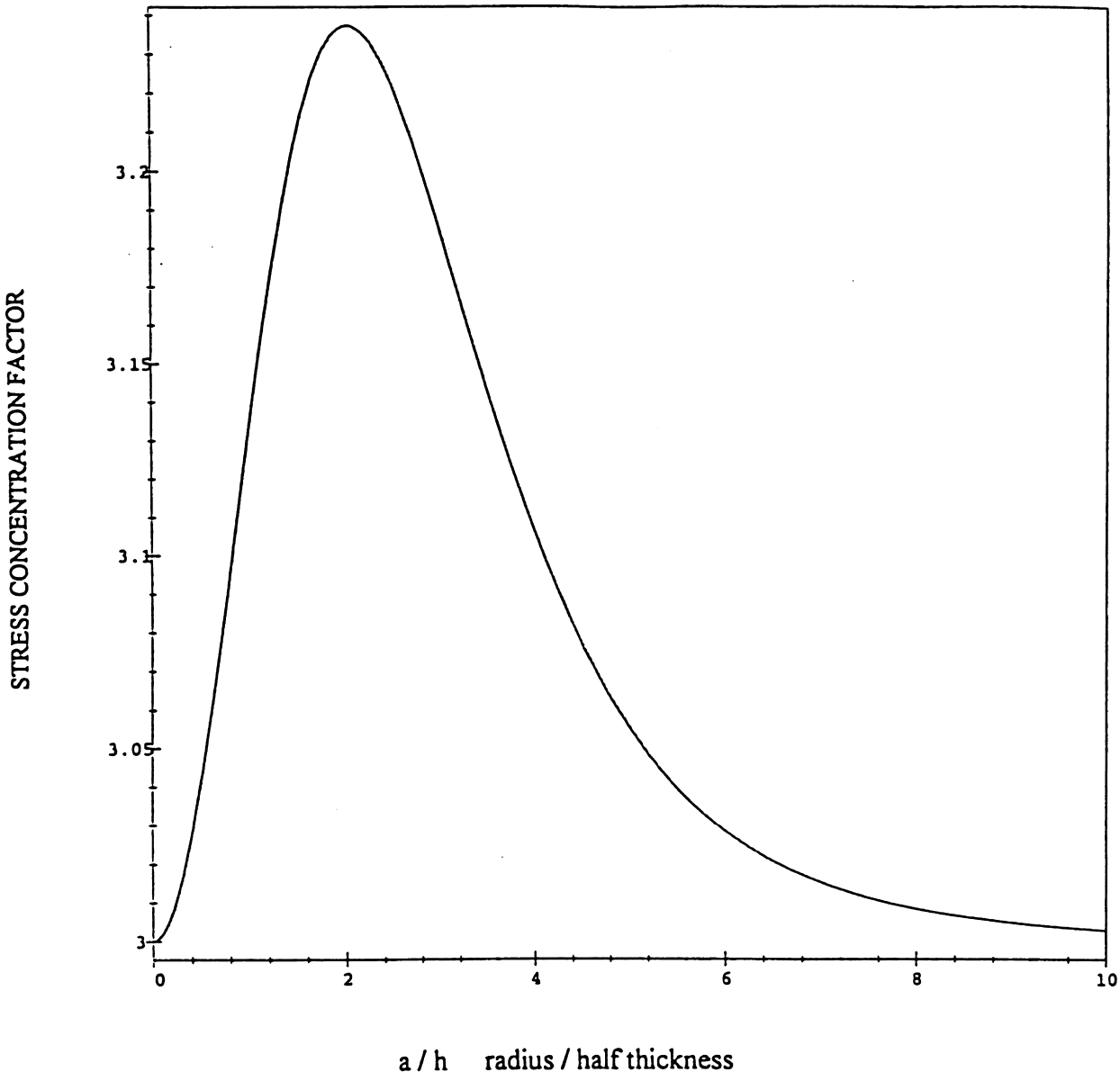

Fig. 5. Maximum stress concentration factor versus diameter to thickness ratio.

introduced by the rapid impact of a knife-edge. The crack resembled a very sharp ellipse with crack tips sharp enough to represent a crack. Subsequently, the vessels were sealed internally with a thick hard rubber sheet, in the area of the crack, and were then pressurized incrementally with pressure differentials of 5 psi. This incremental 'pressure stepping' clearly suggests that the bending and bulging effects may no longer be neglected since they represent a cumulative effect.

Let us examine next, how well can one predict the failing pressures for the UCSD static tests #1 and #2. A closer examination of the geometrical and loading characteristics of test #1 reveals that, because λ is greater than 5.5 and because the bending effects present are not negligible, one must use the general failure criterion by including the pertinent bending terms which in this case are significant. In view of this, Eq. (6) now becomes

$$\frac{q_0}{1000}\,\frac{R}{h}\sqrt{\pi c}F(\lambda) = K \tag{7}$$

where

$$F(\lambda) = \left\{ f_e(\lambda) + f_b(\lambda)\frac{\sigma_{\text{appl.bend}}}{\sigma_{\text{appl.hoop}}} \right\} \tag{8}$$

and $f_e(\lambda)$, $f_b(\lambda)$ are given numerically in the above reference. Without going into the numerical details (Appendix D), the predicted results for tests #1 and #2 become, respectively:

General data: $2R = 20.75$ in., $2c = 5.5$ in.

UCSD static test #1: For test #1, $h = 0.05$ in. and $h/c =$

0.02, and from Fig. 4 one reads a value of K that is closest to that thickness. In this test using $K = K_{\text{lower}} = 62$ ksi in. and $q_0 = 31.2$ psi. The failing pressure reported was 34.4 psi.

It should, furthermore, be noted that for the UCSD test #1, the hard rubber sheet used to seal the crack was well bonded to the interior surface of the vessel. Consequently, the rubber did carry some load and this was substantiated after the failure since it fractured along the same direction of the crack and at a 45° plane through its thickness. In carrying out test #2, however, the rubber sheet was not bonded to the vessel. We have estimated the load carrying capacity of the rubber sheet for test #1 to be approximately 1.6 psi. Thus, accounting for the rubber (see Appendix E), we predict a failing pressure for test #1 to be, approximately, 32.8 psi.

UCSD static test #2: For test #2, $h = 0.086$ in. and $h/c = 0.03$, and from Fig. 3, one reads a value of K that is closest to that thickness. In this test using $K = K_{\text{lower}} = 65$ ksi in. and $q_0 = 59.6$ psi. The failing pressure reported was 59.9 psi.

Perhaps it is appropriate here to emphasize that in both UCSD tests the upper and lower faces of the crack were not touching.

6. Conclusions

Although the correlation function (Eq. (3)) was derived on the basis of a homogeneous and isotropic material, the author believes that it reflects the dominant term of a geometrical inherent property that exists between shell structures and similarly loaded flat plates of the same material. Needless to say that such a property is of great practical significance to the designer for, it is now possible to successfully predict catastrophic failures in cylindrical structures from experimental data accumulated in the laboratory on flat plates. This is an advantage that has not only important economic implications but also the experiments that need to be carried out are much simpler.

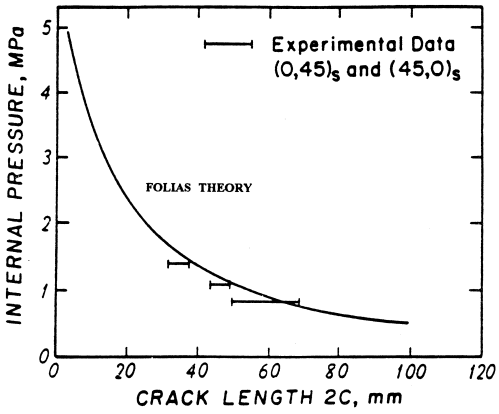

Fig. 6. Comparison between theory and experiment for graphite/epoxy cylinders with axial slits.

Comparison between the theoretically predicted values and the experimental UCSD data shows a very good agreement. Further, in order to verify this hypothesis, we will apply it to the case of a composite material. Unlike the fracture of metals, which is well characterized by the principle of linear fracture mechanics, the fracture of composite structures involves a complex interaction of fiber breaks, matrix cracks and interply delaminations.

Without going into the details, we compare in Fig. 6 the results of Eq. (3) with the experimental data available in the literature [12] on pressurized graphite/epoxy cylinders. The cylinders were slit in the longitudinal direction and were pressurized. The agreement is fairly good.

Appendix A

Summary of 2219-T87 Fracture Toughness K Experimental Test Data by Roy Foreman [13].

Specimen number	Thickness h (in.)	Spectral width W (in.)	Initial crack $2c$ (in.)	Failure stress (ksi)	K (in.)
1A	0.19	20.05	8.11	18.52	73.69
2A	0.19	20.05	8.11	18.91	75.18
3A	0.19	20.04	8.07	20.04	79.29
4A	0.19	20.05	8.22	17.85	71.72
5A	0.19	20.05	8.11	17.92	71.29
1B	0.19	9.93	1.04	40.24	51.77
2B	0.19	10.03	1.04	39.78	53.68
3B	0.19	9.97	1.11	42.96	57.11
1C	0.19	10.04	2.15	33.11	62.53
2C	0.19	9.98	2.18	32.21	61.49
3C	0.19	9.98	2.17	32.86	62.48
1D	0.19	10.03	3.64	26.71	69.53
2D	0.19	9.98	3.65	25.41	66.41

(*continued*)

Specimen number	Thickness h (in.)	Spectral width W (in.)	Initial crack $2c$ (in.)	Failure stress (ksi)	K (in.)
3D	0.19	10.02	3.59	25.51	65.86
1E	0.19	9.98	5.13	17.96	61.26
2E	0.19	10.02	5.09	18.49	62.59
3E	0.19	10.04	5.12	18.91	64.24
1F	0.19	3.91	0.65	44.96	46.05
2F	0.19	3.91	0.64	46.01	47.01
3F	0.19	3.91	0.65	43.82	45.01
1G	0.19	3.91	1.16	35.01	49.94
2G	0.19	3.91	1.16	35.01	49.94
3G	0.19	3.91	1.18	35.62	51.36
1H	0.19	3.91	2.16	21.23	48.81
2H	0.19	3.91	2.17	21.29	48.95
3H	0.19	3.91	2.11	21.81	48.92

Appendix B

Specimen number	Thickness h (in.)	Spectral width W (in.)	Initial crack $2c$ (in.)	Failure stress (ksi)	K (in.)
2J	0.08	10.06	2.08	29.71	68.52
2K	0.08	10.01	3.61	21.71	67.58
2L	0.08	10.01	5.08	14.61	60.19

Appendix C

Fracture toughness (test data by Roy Foreman [13])

Test	h/c	K	$2c/2w$
A	0.05	74	0.41
B	0.34	54.00	0.11
C	0.18	62.00	0.22
D	0.10	67.00	0.36
E	0.08	63.00	0.51
F	0.60	46.00	0.16
G	0.33	51.00	0.30
H	0.18	49.00	0.56
2J	0.08	69.00	0.21
2K	0.05	68.00	0.36
2L	0.03	60.00	0.51

Appendix D

Failure criterion

$$\sigma_{\text{hoop}}\sqrt{\pi c}\{f_e(\lambda) + f_b(\lambda)g(\lambda)\} = K; \qquad \lambda < 8$$

where

$$\lambda^2 = \sqrt{12(1-\nu^2)}\left(\frac{c^2}{Rh}\right)$$

$$g(\lambda) = \frac{\sigma_{\text{bending}}}{\sigma_{\text{hoop}}} = \frac{1}{6}\frac{\pi}{64}\lambda^2.$$

For test #1: $f_e(\lambda) = 4.00 - 0.12g(\lambda)$, and $f_b(\lambda) = (-0.12 - 0.22g(\lambda))3.33$.For test #2: $f_e(\lambda) = 3.21 - 0.11g(\lambda)$, and $f_b = (0.02 - 0.23g(\lambda))3.33$.

Remark: When no bending is present, the criterion may be approximated by the simple relation:

$\sigma_{\text{hoop}}\sqrt{\pi c}\sqrt{1 + 0.317\lambda^2} = K; \qquad \lambda < 8.$

Appendix E

Estimate of load carried by rubber seal

APPENDIX E

ESTIMATE OF LOAD CARRIED BY RUBBER SEAL.

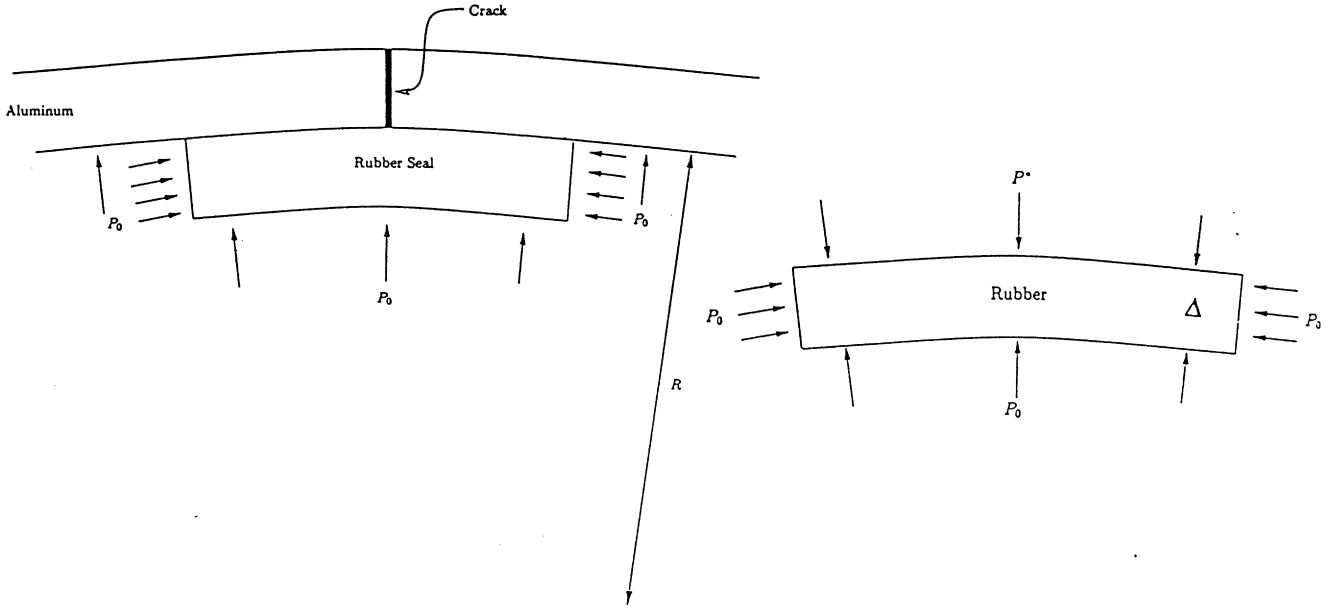

p_o = internal pressure

p^* = normal pressure between rubber and aluminum vessel

Equilibrium of rubber segment implies :

$$p_o - \frac{(p_o - p^*)(R-\Delta)}{\Delta} = 0 ,$$

or

$$p^* = (1 - \tfrac{2\Delta}{R})/(1 - \tfrac{\Delta}{R})p_o = (1 - \tfrac{\Delta}{R})p_o + O(\Delta^2)$$

For $\Delta = 0.50in.$, $R = 10.40in.$

$$p^* = (1 - \tfrac{0.50}{10.40})p_o = 0.95p_o,$$

hence the aluminum vessel experiences, locally, a pressure equal to $0.95p_o$, and

$$p_{fail} = \frac{31.20}{0.95} = 32.80 \quad psi.$$

where p_0 is the internal pressure and $p*$ the normal pressure between rubber and aluminum vessel.

The equilibrium of rubber segment implies:

$$p_0 - \frac{(p_0 - p^*)(R - \Delta)}{\Delta} = 0$$

or

$$p^* = \left(1 - \frac{2\Delta}{R}\right) / \left(1 - \frac{\Delta}{R}\right) p_0 = \left(1 - \frac{\Delta}{R}\right) p_0 + O(\Delta^2).$$

For $\Delta = 0.50$ in. $R = 10.40$ in.

$$p^* = \left(1 - \frac{0.50}{10.40}\right) p_0 = 0.95 p_0,$$

hence the aluminum vessel experiences, locally, a pressure equal to $0.95p_0$, and

$$p_{\text{tail}} = \frac{31.20}{0.95} = 32.80 \text{ psi}.$$

References

[1] Folias ES. An axial crack in a pressurized cylindrical shell. Inter_national Journal of Fracture Mechanics 1965;1:20–46.

[2] Folias ES. Fracture in pressure vessels. In: Fung YC, Sechler E, editors. Thin shell structures 1974, chap. 21.

[3] Allen FC. Effect of thickness on the fracture toughness of 7075 aluminum in the T6 and T73 conditions. ASTM STP 1971;486: 16–38.

[4] Feddersen CE et al. An experimental and theoretical investigation of plane stress fracture of 2024-T351 Al-alloy. Battelle Columbus Report, 1970.

[5] Broek D. The residual strength of light alloy sheets containing fatigue cracks. Aerospace proceedings, London: Macmillan, 1966. pp. 811–835.

[6] Christensen RH, Denke PH. Crack strength and crack propagation characteristics of high strength materials. ASD-TR-61-207, 1961.

[7] Weiss V, Yukawa S. Critical appraisal of fracture mechanics. ASTM STP 1965;381:1–29.

[8] Tetelman AS, McEvily AJ. Fracture of structural materials, New York: Wiley, 1967.

[9] Folias ES, Wang JJ. On the 3D stress field in a plate weakened by a hole. International Journal of Computational Mechanics 1990.

[10] Folias ES. Private communication.

[11] Folias ES. Journal of Applied Mechanics 1975;42(3):663–674.

[12] Graves MJ, Lagace PA. Composite Structures 1985;4:75–91.

[13] Foreman R. Private communication, 1995.

[14] Reference deleted.

[15] Penado FE, Folias ES. The 3D stressfield around a cylindrical inclusion in a plate of arbitrary thickness. International Journal of Fracture Mechanics 1989;39:129–146.

[16] Marguerre K. Zur theorie der gekrummten plattegrosser Formanderung. In: Proceedings of the 5th International Congress on Applied Mechanics. 1938. pp. 93–101.

[17] Copley LG, Sanders JL. Longitudinal crack in a cylindrical shell under internal pressure. International Journal of Fracture Mechanics 1969;5:117–131.

[18] Erdogan F, Kibler J. Cylindrical and spherical shells with cracks. International Journal of Fracture Mechanics 1969;5:229–237.

[19] Folias ES. Private communication, 1997.